Study on Acoustic Prediction and Reduction of Epsilon Launch Vehicle at Lift-off

S. Tsutsumi,[1]
JAXA, Sagamihara, Kanagawa, 252-5210, Japan

T. Ishii[2]
JAXA, Chofu, Tokyo, 182-8522, Japan.

K. Ui[3]
JAXA, Tsukuba, Ibaraki, 305-8505, Japan

S. Tokudome[4]
JAXA, Sagamihara, Kanagawa, 252-5210, Japan

and
K. Wada[5]
Science Service Inc.,Chuuou-ku, Tokyo, 103-0012, Japan

Subscale model tests and a numerical investigation are performed to predict and attenuate acoustic level of the Epsilon launch vehicle at lift-off. Requirements for the subscale model test to predict a full-scale acoustic environment are investigated, and then, the scale size of the model test is set at 1/42. The launch pads employed herein are designed to attenuate reflection of the Mach wave radiated from the free jet and the acoustic wave due to the jet's impinging on the flame deflector. When comparing the acoustic result taken at the fairing location with that at three different altitude, $9D_e$, $14D_e$, and $22D_e$, where D_e represents the nozzle exit diameter, the acoustic level observed at $14D_e$ is the highest and exceeds the design requirement at all frequencies. It is revealed from the numerical analysis that the reflection of Mach waves radiating from the free jet within the flame path is dominant acoustic sources. A front cover is attached to the vertical flame path to shield the Mach wave radiation, and 3 dB attenuation

[1] Engineer, JAXA's Engineering Digital Innovation (JEDI) center, 3-1-1 Yoshinodai, AIAA Member.
[2] Associate Senior Researcher, Institute of Aeronautical Technology, 7-44-1 Jindaiji-Higashi, AIAA Member.
[3] Engineer, Space Transportation Mission Directorate, 2-1-1 Sengen.
[4] Associate Professor, Institute of Space and Astronautical Science, 3-1-1 Yoshinodai, Senior Member AIAA.
[5] Researcher, Tokyo Office, 1-3-15 Nihonbashi-Horidome.

in overall sound pressure level is achieved. The design methods and the knowledge obtained in this study are valid for the design of the launch pad to attenuate lift-off acoustics.

Nomenclature

C	=	speed of sound, m/s
C^*	=	critical speed of sound, m/s
D	=	diameter, m
f	=	frequency, Hz
H	=	distance of the nozzle exit from the ground, or ground plate, m
L	=	length scale, m
M	=	Mach number
$\dot{m}$	=	mass flow rate, kg/s
N	=	Fresnel number
P	=	pressure, Pa
ΔP	=	pressure fluctuation from the ambient value, Pa
R	=	radius of microphone arc, m
Re	=	Reynolds number
St	=	Strouhal number
U	=	velocity, m/s
U_c	=	convective velocity of vortex structure, m/s
W	=	overall acoustic power, W
W_{ref}	=	reference acoustic power, 10^{-12} W
X_c	=	core length of jet from nozzle exit, m
X_p	=	location of sound power peak from nozzle exit, m
γ	=	specific heat ratio
δ	=	difference of acoustic propagation path
η	=	acoustic efficiency
θ	=	angle from free jet axis, degree

λ = wave length, m

μ = molecular viscosity, Pa·s

ρ = density, kg/m^3

Subscripts

a = ambient condition

e = nozzle exit condition

full = full-scale

j = fully-expanded jet condition

o = chamber stagnation condition

sub = subscale

I. Introduction

PROPULSIVE power generated by rocket engines is so strong that exhaust jets emit an intense pressure wave. The pressure wave propagates to the launch vehicle, causing severe acoustic loading. Prediction and reduction of the relevant acoustic levels is an important design challenge in developing a launch vehicle and a payload. The retired M-V solid launcher generates 3,700 kN of thrust at lift-off, and the overall acoustic power reaches 197 dB. The measured acoustic level outside the fairing was roughly 158 dB in overall sound pressure level (OASPL). [1] The development of the Epsilon launch vehicle to succeed the M-V requires reduction of the acoustic levels. The standard configuration of the Epsilon is composed of a three-staged solid rocket, and can launch a 1,200 kg payload into low earth orbit. The required acoustic level outside the fairing of the Epsilon is 147 dB in OASPL, even though the overall acoustic power generated by the 1st-stage solid motor with the thrust of 2,000 kN is 194 dB, only 3dB lower than that of the M-V. Moreover, Epsilon launches will need to reuse launch pad components from the M-V such as the rocket assembly tower and the boom, as shown in Fig. 1. This requirement also implies that a water injection system for noise reduction cannot be employed.

NASA SP-8072 [2] has been referenced to predict the acoustic levels of launch vehicles during lift-off. NASA SP-8072 describes an empirical method based on flight data and firing tests. Acoustic parameters, such as source power distribution, frequency distribution, and directivity, are modeled based on the characteristics of the free jet. They are distributed along the jet flow over the launch pad. It is evident that the acoustic mechanism is not the same as that of

the free jet, when the exhaust jet impinges on a flame deflector. In NASA SP-8072, the effect of jet impingement on the flame deflector is included in the acoustic efficiency calculation. Many studies have been carried out to improve upon the method described in NASA SP-8072. Varnier reports that the length of the jet core proposed by Eldred et al. should be reduced, based on acoustic measurements. [3] On the other hand, Horne et al. and James et al. have recently shown the validity of Eldred's modeled jet core length. [4,5] Jet core length is directly correlated to the source power and frequency distributions, so that modeling the jet core length is one of the key issues in NASA SP-8072. However, the discussion remains open. Directivity is also a key parameter with great impact in NASA SP-8072. Haynes and Kenny compare the measured directivity of static firing tests using a full-scale solid motor and the model of Eldred et al. [6] Considering the effects of the flame deflector, Varnier implements the empirical model in the case of jet-plate interaction. [7] Koudriavtsev and Safronov propose another empirical model based on detailed measurements of the jet's impingement on practical deflectors. [8] Acoustic propagation is another issue for consideration. Spherical wave propagation from each point source distributed along the flow path is assumed in NASA SP-8072, but it is difficult to evaluate the effect of reflection and diffraction caused by complex launch pad structures. Plotkin introduces both the effects of reflection and diffraction into the sound propagation model within NASA SP-8072. [9] Casalino et al. employs Computational AeroAcoustics (CAA) to evaluate acoustic propagation from the noise sources by an empirical method. [10]

Even though all these studies have been conducted to improve the prediction accuracy of the empirical method, the prediction accuracy so far demonstrated is insufficient, because the acoustic mechanism is not yet clearly understood. Acoustic measurements using subscale models are essential for the development of the launch pad. [11-15] 1/20-scale tests are performed in the development of the Ares I, Ariane 5, and VEGA launch vehicles. In addition, simplified model tests using a hot jet generated from a hydrogen-air combustor are conducted for the Ariane 5 and VEGA at the MARTEL facility. Since each test at the MARTEL facility can be conducted easily, the flame duct and water injection system are designed. [13,14] Recently, phased array having several tens of microphones is used to identify the acoustic source distribution. Such result also supports the design of the launch pad to attenuate acoustic level at lift-off. [13,15] Tsutsumi et al. apply Computational Fluid Dynamics (CFD) based on an implicit Large-Eddy Simulation (LES) to investigate the acoustic generation mechanism for the Japanese launch vehicles. [16, 17] Acoustic waves emanating from the jet that impinges on the deflector are also studied numerically, and the shape of the deflector to reduce the acoustic level is discussed. [18] Nonomura et al. investigate the acoustic mechanism for a cold jet having

M_e=2.0 impinging to a 45-degree-inclined flat plate by using implicit LES. [19, 20] Tsutsumi et al. and Akamine et al. also carry out both numerical and experimental studies in order to understand a M_e=1.8 cold jet impinging to inclined flat plates. [21, 22] CFD is a useful tool for analyzing the mechanism of acoustics, and is extensively employed in the development of the Epsilon launch vehicle. 1/42-scale model test is also conducted for obtaining an acoustic level with sufficient accuracy. This study discusses requirements for the subscale model acoustic prediction test, as well as methods to predict a full-scale acoustic environment based on the subscale result in section II. In the section III, setups for the test stand and measurement system are briefly explained with a discussion of error estimations and the reliability of acoustic results. Based on findings in the previous studies, launch pads tested in this study are designed to decrease the acoustic level of the vehicle. In section IV, ideas to attenuate acoustic waves propagating to the vehicle are proposed. The CFD tool employed in this study is shown in section V with a validation study using experimentally obtained microphone data. In section VI, the acoustic field is discussed based on the microphone results, and further techniques for acoustic attenuation is analyzed by with CFD and is examined quantitatively in the subscale test.

II. Requirements for Subscale Tests and Prediction of Full-scale Acoustics

A subscale model test is necessary for obtain an acoustic level with sufficient accuracy, but requirements for the subscale test, such as scale size, are not obvious that will generate the same acoustic spectrum as that of the practical launch environment. Acoustic generation and propagation should be considered separately to clarify the requirements for the subscale model test.

The Reynolds number and the Strouhal number based on the nozzle exit are a key parameter for the acoustic generation, and should be made identical between the subscale test and the full-scale environment in order to obtain the same acoustic features.

$$\mathrm{Re} = \rho_e U_e D_e / \mu_e \tag{1}$$

$$\mathrm{St} = f D_e / U_e \tag{2}$$

However, the relationship between the nozzle exit velocity, U_e, and the nozzle exit diameter, D_e, indicates that the same Reynolds number and Strouhal number cannot be obtained in the subscale test and the full-scale environment. The acoustic spectrum can be normalized by the Strouhal number, if the Reynolds number for the subscale test is

chosen carefully. The shadowgraph of a cold jet with M_e=2 is shown in Fig. 2. The figure displays clear Mach wave radiation. The Mach wave radiation is one of the dominant mechanisms for acoustics during lift-off of the launch vehicle. [16,23] Troutt and McLaughlin show the effect of the Reynolds number on the acoustic spectrum of cold jets having M_e=2. [24] The result of the lowest Re number (7900) shown in Fig. 3(c) shows a distinct peak at St=0.2 since the vortex structure corresponding to that size becomes dominant. Comparing the results of higher Reynolds numbers shown in Figs. 3(a) and (b), almost identical spectra are obtained. The comparison shown in Fig. 3 indicates that the Reynolds number of the subscale motor should be greater than roughly 10^5. Acoustic diffraction and reflection due to launch-pad structure and ground surface are major issues for consideration. Maekawa's thin screen acoustic shielding model is well known for effective acoustic diffraction. In that model, the attenuation level due to diffraction is normalized by the Fresnel number, $\mathrm{N} = 2\delta/\lambda$, where δ represents the difference between the directed and diffracted acoustic propagation paths. [25] It has also been shown that perfect reflection of the acoustic wave can be normalized by the Fresnel number. [26] Therefore, the following equation is derived from the Fresnel number in order to equalize the same characteristics of acoustic propagation between the sub- and full-scale models.

$$\delta_{full}/\lambda_{full} = \delta_{sub}/\lambda_{sub} \tag{3}$$

Therefore, the following relationship is derived.

$$f_{full}L_{full} = f_{sub}L_{sub} \tag{4}$$

Note that difference of the path, δ, is replaced by L, representing the length scale of the model. Comparing Eqs. (2) and (4), it is derived that the exit velocity of the subscale motor should be equal to that of the full-scale motor when the acoustic spectrum can be normalized by the Strouhal number.

Directivity is another issue that should also be considered in designing the subscale test. The directivity angle of the Mach wave from the jet axis can be derived from the convective velocity of the vortex structure and the ambient sound velocity.

$$\theta = \cos^{-1}(C_a/U_c) \tag{5}$$

The convective velocity is expressed as $U_c = KU_e$ where K is a constant and estimated to be between 0.5 and 0.7. [27] Assuming that the constant K is the same value regardless of the size of the motor, the Eq. (5) indicates that two jet having identical exit velocity result in the same directivity. Therefore, requirements for the subscale model test are as follows; 1) the Reynolds number based on the nozzle exit exceeds 10^5 and 2) the exit velocities of the jets are equal.

According to Varnier [3], overall acoustic power level is estimated with:

$$W = \eta \frac{1}{2} \dot{m} U_j^2 \tag{6}$$

The acoustic efficiency is evaluated based on following equation. [3, 28]

$$\eta = 0.0012 \left(\frac{\gamma_j}{\gamma_a}\right) \left(\frac{C^*}{C_a}\right)^3 \left(\frac{C^*}{U_e}\right)^2 \tag{7}$$

According to Eq. (7), keeping acoustic efficiency constant depends on the propellant and combustion conditions, such as chamber pressure, chamber temperature, and the area ratio of the nozzle being the same between the sub- and the full-scale motors. Moreover, U_j will also be equal under the above conditions. The following relationship for the overall acoustic power level results.

$$W_{full} = \left(\frac{\dot{m}_{full}}{\dot{m}_{sub}}\right) W_{sub} \tag{8}$$

The ratio of the mass flow rate can be reduced to the square of the length scale ratio. Therefore, Eq. (8) can be rewritten as follows:

$$W_{full} = \left(\frac{L_{full}}{L_{sub}}\right)^2 W_{sub} \tag{9}$$

Assuming that the acoustic wave propagates spherically, sound pressure level (SPL) is evaluated from:

$$\mathrm{SPL} = 10 \log\left(\frac{W}{W_{ref}}\right) - 10 \log(4\pi R^2) \tag{10}$$

The second term in the right hand side of Eq. (10) indicates the distance law of the acoustic propagation, and the difference between motor scales is expressed as $10 \log\left(L_{sub}/L_{full}\right)^2$. Consequently, Eqs. (9) and (10) show that SPL_{sub} is equivalent to SPL_{full}. According to Eq. (4), which is valid for subscale tests having appropriate Re and exit jet velocity as discussed above, a relationship for the frequencies is derived easily as follows:

$$f_{full} = \left(\frac{L_{sub}}{L_{full}}\right) f_{sub} \tag{11}$$

Equation (11) explains that the acoustic wave measured from the subscale test has a higher frequency-to-scale ratio than that of the full-scale environment. The derived Eqs. (9) and (11) agree with Dougherty and Guest's findings in their study of the space shuttle environment based on a 6.4% scale model test. [11]

In order to predict the full-scale acoustic environment based on the subscale results, the error associated with the difference between sub- and full-scale conditions should be estimated. When the acoustic wave propagates in air, acoustic energy is absorbed due to the viscosity of the air. According to Eq. (4), the wave length for the subscale model is shorter than that of the full-scale model, thus larger attenuation appears in the subscale test. The effect of air absorption estimated based on reference [29] is shown in Fig. 4. Propagation distance is set to $60D_e$ here, and

attenuation levels between full-scale and 1/42-scale environments are compared. At St=0.5 (f_{full}=790 Hz), for example, the attenuation level of the subscale model is estimated to be 1.8 dB larger than that of the full-scale environment. Ambient temperature distribution causes non-uniform speed of sound in the air, resulting in the refraction of acoustic waves. [30] The refraction may also be a source of error, and the effect is remarkable in higher frequency regions. Target frequency in the full-scale launch vehicle reaches 2 kHz. Considering a 2 kHz acoustic wave propagating 40 m in the air with a gradient in the speed of sound of ±0.3 1/s, the difference due to refraction is estimated to be roughly 3 dB. Therefore, the effect of acoustic refraction is not negligible. In reality, temperature distribution of the ambient air around the launch vehicle is too complicated to estimate analytically because of the convection and radiation from hot exhaust jets. Much care should be paid to the error attributed to the acoustic refraction when the full-scale acoustic level is predicted based on subscale measurements. [28] The discussion here shows the examples of the error. Further discussion will be carried out when the subscale results is compared with the flight data.

III. Subscale Model Test

The Subscale Measurement for Acoustic Prediction (SMAP) testing campaign is conducted at the Noshiro Rocket Testing Center. 15 solid motors are used during the SMAP testing campaign. Figure 5 shows a schematic of the test stand. A subscale solid motor representing the 1st stage of the Epsilon launcher is attached to a load cell to measure thrust, and then, the load cell is attached to a hydraulic cylinder to change the motor height. The hydraulic cylinder is suspended from the ceiling of the stand. A subscale launch pad is mounted on the square steel plate with $50D_e \times 50D_e$ size representing the ground surface. Acoustic absorption material is wrapped around the test stand, the hydraulic cylinder, and microphone arcs to prevent reflection.

A. Specifications of Subscale Motor

Subscale motors having similar propellant to the 1st stage motor of the Epsilon are employed in the SMAP testing campaign. Considering the requirements for the subscale motor, the nozzle is designed to obtain the appropriate exit velocity. A motor scale of 1/42 is selected. The Reynolds number based on the nozzle exit results in 2.2×10^5, which meets the requirement discussed in section II. Jet parameters are listed in Table 1. Typical time history of P_o and thrust are shown in Fig. 6. Working time is roughly 2 s, and the acoustic data is extracted from 0.25 s to 2.0 s where P_o nearly shows a plateau. The thrust shown in Fig. 6 shows a similar profile as the P_o, and the thrust at the plateau region

is roughly 1 kN. Based on Varnier [3], the core length of the jet of the subscale motor is estimated to be $X_c = 1.75D_j\left(1 + 0.38M_j\right)^2 = 6.7D_e$, and the location of the sound power peak supposed to originate in the Mach wave radiation from the free jet is calculated to be $X_p \approx 1.5X_c = 10.0D_e$. [2] Note that change of the nozzle exit diameter during the firing of 2 s is negligible, so that D_e is fixed to the designed value in this study.

B. Acoustic Measurement Setup

1/4 inch condenser microphones, GRAS 40BP, are employed with rain protection caps, GRAS RA0127. Locations of the microphones are shown in Fig. 7. Far-field acoustics are measured with a microphone arc of 6 microphones separated by 10-degree increments at a radius of $60D_e$ from the impingement point. An additional 3 microphones are located $11D_e$ upward from the nozzle exit plane to measure the acoustic environment around the faring of the Epsilon launch vehicle. These three microphones are distributed circumferentially to the west, south, and east directions. Figure 8 shows a typical Power Spectrum Density (PSD) plot. A bumpy spectrum appeared at frequencies over 30 kHz. According to the preliminary study in the anechoic chamber, this spectrum must be attributed to the rain protection cap, not the physics of the system. Therefore, the measured acoustic spectrum up to 30 kHz, corresponding to 710 Hz at full-scale, is considered for the discussion below.

Error included in the obtained acoustic data is discussed below. The surface of the microphones are located parallel to the direction of acoustic wave propagation in order to minimize error due to the incidence angle of acoustic waves. According to the data sheet for GRAS 40BP, the error at the maximum f_{sub} = 30 kHz is roughly ±0.5 dB. Figure 4 shows that error originating in the acoustic wave propagation through the air is 1.5 dB at St= 0.46 (f_{sub} = 30 kHz). These two errors total combine to be about 2.0 dB.

Since the SMAP testing campaign is conducted in an open field, the repeatability of the acoustic results must be verified. During the SMAP testing campaign, an additional two tests are conducted. In these tests, a 45-degree-inclined flat plate is located $10D_e$ downstream from the nozzle exit, and far-field acoustics data is measured by 14 microphones separated by 6-degree increments at a radius of $60D_e$ from impingement point as shown in Fig.9. These two tests are conducted day by day. Difference of the OASPL and the 1/1 octave-band SPL between those two tests are compared in Fig. 10. The difference observed is 0.8 dB in OASPL, and 1.2 dB at St=0.008 in 1/1 octave-band SPL. These results show that the acoustic measurements reported here have sufficient repeatability even in open-field tests. Therefore, only one firing is done for each condition in the SMAP testing campaign.

C. Verification of Acoustic Measurement

Acoustic data for the free jet condition of the 1/42 scale motor is measured, and it is compared with results from a static-firing test of a 260-kN solid motor having roughly 1/3 scale [31] to clarify that the 1/42 scale motor is sufficient for acoustic testing. The 260-kN solid motor is set on the ground, and the jet is exhausted horizontally. 5 microphones are located at a radius of $63.5D_e$ from the nozzle exit as shown in Fig.11(a). However, the 1/42-scale motor is lifted up vertically by the hydraulic cylinder to $50D_e$ above the square steel plate, and the jet is exhausted downward. The configuration of the microphone arc for the free jet case in the SMAP testing campaign is different from Fig. 7. As shown in Fig.11(b), 11 microphones are attached with 10-degree increments at a radius of $60D_e$. The result taken in the static-firing test of the 260-kN solid motor is scaled to a radius of $60D_e$ with Eq. (10). A comparison of the OASPL distribution is shown in Fig. 12(a). Except for the microphone at θ=20 degree, the difference in the OASPL turns out to be roughly 3 dB, and the location of the peak values appearing at around θ=50 degree agree reasonably. It is deduced that the effect of the jet deflected by the square steel plate located $50D_e$ downstream from the nozzle exit as shown in Fig.11(b) appears in the result of the microphone at θ=20 degree. The PSD spectrum at θ=50 degree is compared in Fig. 12(b). Though the result of the 260-kN solid motor shows higher value at St=0.005 to 0.1 due to ground reflection, the peak of the spectrum appears at St=0.02-0.4 in both results, and the general characteristics of the spectrum agree reasonably. The comparison here proves that the 1/42-scale motor employed is acceptable for acoustic measurements to predict full-scale conditions.

IV. Acoustic Design of Launch Pad

Preliminary design of a launch pad for the Epsilon launch vehicle is described below, based on knowledge obtained from previous studies and CFD. As described in section I, the Epsilon launch vehicle is required to reuse the launch pad components of the retired M-V, such as the rocket assembly tower and the boom, as shown in Fig. 1. Within the restrictions due to this existing launch complex of the retired M-V launcher, preliminary design of a launch pad for the Epsilon begins with the configuration shown in Fig. 13. It is similar to that used with the Minotaur I launch vehicle at the NASA's Wallops Flight Facility. The launch vehicle is set on the launch deck. Impinging on the flame deflector, the jet flows downstream on the ground. Figure 14 shows the dominant acoustic sources analyzed from the previous studies. When the vehicle is close to the flame deflector, acoustic waves radiated from the jet impinging on the flame

deflector and the Mach wave radiation from the wall jet, as shown in Fig. 14(a), are dominant. [17-22] The acoustic wave due to the jet impingement propagates omnidirectionally from the vicinity of the impingement region, and determines the acoustic environment surrounding the vehicle. On the other hand, the Mach wave radiation from the wall jet has a strong directivity at roughly 50 degree from the wall jet axis, so that the effect on the vehicle must be small. As the vehicle climbs, Mach wave radiation from the free jet becomes relevant. As shown in Fig. 14(b), the Mach wave propagates obliquely downstream, and impinges on the ground. The Mach wave then reflects from the ground back onto the vehicle. [16] X_p in the present subscale motor is $10.0D_e$, so that H=$10.0D_e$ is considered to be the boundary between the acoustic waves due to the jet impingement and the Mach wave radiation from the free jet. In the following discussion, distance of the nozzle exit normalized by the nozzle exit diameter, H/D_e, is used to distinguish which acoustic source is dominant. In order to reduce the acoustic waves due to the jet impingement to the flame deflector, the inclination angle of the flame deflector should be steep for the region where the jet impinges, and rapid change in the contour should be avoided. [18,21] The surface area of the launch deck should be minimized in order to reduce the reflection of the Mach wave radiation from free jet. In addition, the launch deck should be located as high as possible from the ground surface in order to increase the propagation distance of the Mach wave. Parametric study using CFD for preliminary design is conducted to investigate sensitivity to the height of the launch deck. [32] The deflector shape and configuration of the launch pad are determined as shown in Fig. 15. The launch deck is changed to a ring-shaped mount to minimize surface area. The height of the ring shaped mount is set to $8D_e$ due to the limitations of the existing rocket assembly tower shown in Fig. 1. The boom to which the vehicle is attached is also pictured in Fig. 15. The flame deflector of the M-V launch vehicle is redesigned to have an initial inclination angle of 14 degree from free jet axis, with the contour smoothly changing to meet the ground. Detailed design begins with the baseline configuration of Fig.15(a) having an open flame path, while front cover is attached to other configuration shown in Fig. 15(b). The rationale for effect of the front cover will be discussed in the section VI.

V. Numerical Method

Since it is difficult to understand the acoustic mechanism from the experiment and the empirical methods alone, CFD technique based on a cell-centered finite-volume method on a multi-block structured grid is employed. The turbulence modeling is an important issue for the aeroacoustic simulation, and a zonal hybrid of LES and Reynolds

Averaged Navier-Stokes (RANS) methods is employed in this study. The turbulent boundary layer on the solid wall is modeled by the RANS based on the Spalart-Allmaras model [33], and the off-wall region is computed by the LES using the standard Smagorinsky model. The eddy viscosities evaluated separately by the RANS and LES models are blended smoothly with a hyperbolic-tangent function. Since the time step is limited by the smallest grid size on the solid wall and the low-frequency wave of 31.5 Hz in the 1/1 octave band is focused, an implicit method based on the Matrix-Free Gauss-Sidel scheme [34] is used for time integration with Newton-Raphson sub-iteration. Second-order temporal accuracy is guaranteed by the three-point backward differencing formula. Since the target is aeroacoustics but the flow contains shock waves, a higher-order scheme with shock-capturing features is required for the convective terms. 6th-order compact differencing scheme [35] is used with a 10th-order low-pass filter [36]. Shock waves are detected by the method proposed by Visbal and Gaitonde [37], and then those regions are evaluated with the Simple Low-dissipation AUSM (SLAU) scheme [38] using 2nd-order Monotone Upstream-centered Scheme for Conservation Laws (MUSCL) interpolation in place of the compact differencing scheme. The Ffowcs Williams-Hawkings (FW-H) acoustic analogy [39] is employed for calculating the propagation of the acoustic wave to the far-field.

Validation and verification of the computational code are performed extensively by comparing the measured results of the M_e=1.8 perfectly expanded cold impinging jet taken by Nakanishi et al. [21,22,40], and measured results taken in the SMAP testing campaign for the free jet, impinging jet on the 45-degree-inclined flat plate, and practical launch pad configurations. In this report, a validation study using the microphone results measured of the practical launch pad configuration shown in Fig. 15(a) is only discussed. The validation study is conducted at H/D_e=14. The computational grid has about 100 million points, and the acoustic cut-off frequency results in St=0.48 (f_{full}=740 Hz). It took approximately two months using 1280 cores of JAXA's supercomputer system, Fujitsu FX1, to resolve down to St=0.012 (f_{full}=20 Hz). The OASPL and PSD spectrum taken from the far-field microphones (Fig. 7) are compared in Fig. 16. According to the discussion in Section III B, error bounds of ±2 dB are superimposed in Fig.16 (a). Both results show a peak in the OASPL at θ=150 degree, and the features of the plots are in good agreement. The prediction accuracy is found to be 4 dB in OASPL. PSD spectra are compared at M2 (θ=120 degree) and M5 (θ=150 degree) as shown in Figs. 16(b) and 16(c), respectively. General features of the spectra agree reasonably at both locations. Both numerical and measured results at M2 show a near-plateau profile at St<0.23, and decrease at higher frequencies. At M5, the microphone data and the numerical analysis show a peak at St=0.045 and 0.023, respectively. Although the

numerical result shows good agreement with the microphone data, the predicted acoustic level overestimates at all microphone locations. According to past CFD studies on the free jet, numerical results tend to show higher level than the microphone measurements especially at the major acoustic emission direction. [41-43] If the resolution of numerical method and computational grid are insufficient, turbulent structure of the jet shear layer contains higher energy at low frequencies than the physics, and obtained acoustic level results in the overestimation. According to Cacqueray et al. [41], simulation of a high-Mach number hot jet should be taken into account the non-linearity in calculating acoustic propagation. Without considering the non-linear propagation effect, obtained acoustic level tends to show higher level. Therefore, the overestimation observed in Fig.16 is caused by the insufficient resolution of the present computation and the FW-H method used for calculating the propagation.

VI. Acoustic Results and Discussions

A. Acoustic Field of Free Jet

The acoustic field of the free jet at far-field arc locations taken in the SMAP testing campaign as shown in Fig.11(b) is discussed before going to the analysis of the acoustic environment around the practical launch pad. The OASPL plot at R=60D_e is shown in Fig. 12(a), and the PSD spectrum at θ=30, 50, 90, and 120 degree at R=60D_e are in Fig. 17. Figure 12(a) shows that the peak of the OASPL appears at around 50 degree, which indicates typical characteristics of the Mach wave radiation from high-temperature and high-Mach-number supersonic jets. The PSD spectrum at θ=30 degree shows peak value at St=0.015, and the peak location increases to higher frequencies as the angle from the jet axis increases. At θ=90 degree and 120 degree, the PSD shows a near-plateau profile and features of the broadband shock-associated noise are not observed.

B. Effect of Distance from Ground on Far-field Acoustics

Acoustic results obtained by the far-field microphones for the baseline configuration of Fig.15(a) are compared in Fig. 18. In this figure, the distance of the nozzle exit from the ground plate changed from H/D_e=9 to 22. At H/D_e=9, the nozzle exit plane is so close to the flame deflector that the dominant acoustic source is the acoustic wave generated from the jet impingement and the Mach wave radiated from the wall jet, as explained in Fig.14(a). On the other hand, the Mach wave radiation from the free jet, as shown in Fig.14(b), is dominant at H/D_e=22. In the case of H/D_e=14,

those two acoustic sources are mixed, since X_p for the present subscale motor is estimated to be $10.0D_e$. It is observed from the OASPL plot in Fig. 18(a) that the case of H/D_e=9 exhibits the lowest OASPL value, and that the OASPL value increases as the solid motor goes upward. Peak of the OASPL at H/D_e=9 and 14 appears at around θ=140 degree to 150 degree, because the dominant acoustic source in these two cases is the Mach wave radiation from the wall jet whose directivity is 50 degree from the wall jet axis. On the other hand, no notable peak appears for the case of H/D_e=22, where the Mach wave radiation from the free jet is the dominant source of the acoustic wave. PSD spectra observed at θ=150 degree, the M5 microphone, at different distances from the ground are compared in Fig. 18(b). The H/D_e=14 case shows higher values than that of the H/D_e=9 case across all frequencies. At the highest altitude case, H/D_e=22, the PSD level is higher than the result of H/D_e=14, except for lower frequencies (St<0.003). A notable hump in the spectrum is observed at 0.02<St<0.05 in the results for H/D_e=14 and 22. The free jet result shown in Fig. 17 indicates that the peak of the Mach wave radiation appears at St=0.01 to 0.05. Therefore, this hump is considered to be related to the reflected Mach wave radiation from the free jet.

C. Acoustic Field around Fairing Location

The measurements for the baseline configuration at H/D_e=14 taken by the three microphones, M7-M9, that are located circumferentially around the fairing location are compared in Fig.19. The M7 is to the west, where the jet is exhausted onto the ground plate, and the M9 is opposite side to M7. The M8 is located to the south. It is observed that the PSD level observed at M7 shows highest value across all frequencies. The lowest level appears for M9, except for the tiny peak appearing at St=0.012. The result of M8 is in the middle. As shown in Fig. 15(a), the flame path is open on the west-facing side, and the jet is exhausted to the west. This explains why the PSD level measured at M7 is highest among the three microphones. It is also observed from Fig. 19 that notable differences related to the microphone placement are observed at higher frequencies, St>0.02, because acoustic waves with higher frequencies are affected by obstacles, such as the launch pad and the vehicle itself. Acoustic tests for the payload fairing are usually conducted in the acoustic diffuse field, but the result shown here indicates that the acoustic load is not circumferentially uniform in practical conditions. In the following discussion, result from the M7 is focused on, because the highest acoustic level among the three circumferentially placed microphones is obtained from the M7.

D. Acoustic Level Attenuation

1/1 octave-band SPLs among three different heights, H/D_e=9, 14, and 22, for the baseline configuration are compared in Fig. 20. Result for the configuration with a front cover as shown in Fig. 15(b) at H/D_e=14 is also included in this figure. The black line in Fig. 20 is the required acoustic level defined during the development of the Epsilon launch vehicle. Results of the subscale tests are scaled to f_{full} according to Eq.(11). Comparing the three different altitude cases, the highest acoustic level is obtained at H/D_e=14. It is observed from result of the H/D_e=9 case that SPL levels at 31.5, 250, and 500 Hz are almost equal to those for H/D_e=14, but a notable difference in SPL is observed at 63.5, and 125 Hz. When the nozzle exit is at a height of $22D_e$ from the ground, the SPL is lower than the other two cases at all frequencies. OASPL levels among three different heights for the baseline configuration are listed in Table 2. Result for the configuration with a front cover at H/D_e=14 is also included in this table. The case of H/D_e=14 shows the highest OASPL value of 149.1 dB. The lowest OASPL value of 141.3 dB is obtained at H/D_e=22. The H/D_e=9 result is in the middle of those two cases, and the OASPL is 147.7 dB. Note that the features observed at the fairing are totally different from the far-field acoustics shown in Fig. 18(a), because the highest acoustic level is obtained at H/D_e=22, and the lowest is at H/D_e=9. The H/D_e=14 result is in the middle of those two cases. It is observed from Fig.20 that the acoustic levels obtained at H/D_e=9 and 14 do not satisfy the design requirement. In particular, the SPL at H/D_e=14 exceeds the required level at all frequency range. The maximum difference is 3.6 dB at 63.5 Hz. It is essential to understand the detailed acoustic mechanism in considering techniques to reduce the acoustic level, so the CFD analysis is applied to the baseline configuration for H/D_e=14. Figure 21(a) shows the flowfield at the symmetry plane visualized by the mean Mach number plot. The thick black line superimposed on this figure indicates the sonic line. The jet exhausted from the nozzle impinges on the flame deflector, and then the wall jet flows downstream. It is found from the sonic line that the wall jet is still supersonic. The Turbulent Kinetic Energy (TKE) plot in Fig. 21(b) makes clear that the free jet shear layer shows higher TKE levels than the wall jet shear layer. The free jet shear layer will then emit major acoustic waves. Figure 21(c) shows the pressure fluctuation at the plane of symmetry. The Mach number plot is also superimposed to visualize the jet flow. It is observed that the free jet shear layer radiates the Mach wave propagating roughly 50 degree downstream from the free jet axis. Because one of the side panels is open in the baseline configuration as shown in Fig. 15(a), the Mach wave also radiates from the free jet within the vertical flame path. The Mach wave propagating obliquely downstream is reflected off the ground, and then turns back to the vehicle. The acoustic wave due to the impinging jet must be one of the acoustic sources, however, it is difficult to find it in

Fig. 21(c). It is deduced that if the Mach wave radiation from the free jet is shielded, the reflected wave propagating upward to the vehicle will be attenuated and the acoustic levels around the fairing reduced. Therefore, the launch pad shown in Fig. 15(b) has a front cover that aims to shield the Mach wave radiation from the free jet shear layer within the vertical flame path. Effect of the front cover is quantitatively investigated in the subscale model test at H/D_e=14. Figure 20 shows that, compared with the result of the baseline configuration, successful attenuation by 2 to 4 dB at all frequencies is obtained. It is also found from Table 2 that the OASPL at H/D_e=14 without the front cover is 149.1 dB, while it is reduced to 146.2 with the front cover. As a result, successful attenuation by 3 dB in the OASPL is achieved. Comparing with the required 1/1 octave-band SPL of the Epsilon launch vehicle, the obtained result by the launch pad with the front cover meets the requirement for H/D_e=14. The PSD spectrum is compared in Fig. 22. Acoustic levels of the launch pad with the front cover are lower than that of the baseline configuration for H/D_e=14 at all frequencies. Notable decrease is observed at St=0.07 in particular. These results indicate that the simple modification of the launch pad can attenuate the acoustic levels once the detailed mechanism of acoustic is understood with the help of the CFD analysis.

VII. Conclusion

A subscale model testing campaign and numerical investigation for the prediction and reduction of acoustic levels for the Epsilon launch vehicle at lift-off are reported. In order to predict a full-scale acoustic environment based on the subscale measurements, this study clarifies requirements for subscale model tests: 1) the Reynolds number based on the nozzle exit of the subscale engine is larger than 10^5 and 2) the exit velocity of the subscale engine is the same as that of the full-scale engine. According to these two requirements, solid motors having 1/42 scale are employed in the testing campaign. The methodology for predicting a full-scale acoustic environment from the subscale model measurement is investigated. Design of the launch pad is discussed to attenuate the Mach wave radiation from the free jet and the acoustic wave generated due to the jet impinging on the flame deflector. It is found that features of the acoustic field change as the nozzle travels upward. Comparing the obtained acoustic data with three different altitudes, H/D_e=9, 14, and 22, acoustic levels observed at H/D_e=14 are the highest, and exceed the requirement of the Epsilon at all frequencies. Numerical results show that the reflection of the Mach wave radiated from the free jet is a dominant acoustic source. In order to attenuate the acoustic level, a front cover is attached in order to shield the Mach wave

radiated from the free jet within the vertical flame path. Successful attenuation is obtained to a degree of 2 to 4 dB in 1/1 octave-band sound pressure level at all frequencies. The acoustic level obtained satisfies the requirement of the Epsilon launch vehicle with only a slight modification of the launch pad. The design methods and the knowledge obtained in this study are valid for the design of the launch pad to attenuate acoustic levels of the launch vehicle at lift-off.

Acknowledgments

The SMAP testing campaign is supported by the technical staff at the Institute of Space and Astronautical Science of JAXA. The authors wish to thank Dr. Kota Fukuda (Tokai University) for discussion of the requirements of subscale tests and the methodology for predicting characteristics of the full-scale acoustic environment.

References

[1] Onoda, J., and Minesugi, K., "Estimation of Mechanical Environment of M-V Satellite Launcher," *Proceedings of the JSASS/JSME Structures Conference, Osaka, Japan,* The Japan Society for Aeronautical and Space Sciences, Tokyo, June 1997, pp.229-232. (in Japanese)

[2] Eldred, K.M., and et al., "Acoustic Loads Generated by the Propulsion System," NASA SP-8072, June 1971.

[3] Varnier, J., "Experimental Study and Simulation of Rocket Engine Freejet Noise," *AIAA Journal*, Vol.39, No.10, 2001, pp.1851-1859.

[4] Horne, W.C., Burnside, N.J., and Panda, J., "Measurements of Unsteady Pressures near the Plume of a Solid Rocket Motor," AIAA Paper 2009-3323, May, 2009.

[5] James, M.M., Salton, A, and Gee, K.L., "Full-scale Rocket Motor Acoustic Tests and Comparison with Models: Updates and Comparisons with SP-8072.", *Journal of the Acoustical Society of America*, Vol.132, No.3, September 2012, pp.1991.

[6] Haynes, J., and Kenny, J., "Modifications to the NASA SP-8072 Distributed Source Method II for Ares I Lift-off Environment Predictions," AIAA Paper 2009-3160, May 2009.

[7] Varnier, J., "Experimental Characterization of the Sound Power Radiated by Impinging Supersonic Jets," *AIAA Journal*, Vol.40, No.5, 2002, pp.825-831.

[8] Koudriavtsev, V.V., and Safronov, A.V., "Noise Generation at Supersonic Jet Interaction with Inclined Deflector," *Proceedings of the 30th International Congress and Exhibition on Noise Control Engineering*, The Hague, The Netherlands, August 2001, pp.139-142.

[9] Plotkin, K., and Vu, B.T., "Extension of a Launch Pad Noise Prediction Model to Multiple Engines and Directional Receivers," *Journal of the Acoustical Society of America*, Vol.132, No.3, September, 2012.

[10] Casalino, D., Barbarino, M., Genito, M., and Ferrara, V., "Hybrid Empirical/Computational Aeroacoustics Method for Rocket Noise Modeling," *AIAA Journal*, Vol.47, No.6, 2009, pp.1445-1460.

[11] Dougherty, N.S., and Guest, S.H., "A Correlation of Scale Model and Flight Aeroacoustic Data for the Space Shuttle Vehicle," AIAA Paper 84-2351, October 1984.

[12] Varnier,J., Piet, J.F., Gely, D., Elias, G., and Radulovic, S., "Modeling of the Acoustic Environment on the Ariane 5 Fairing Using Small Scale," AIAA Paper 96-1721, May 1996.

[13] Gely, D., Elias, G., Bresson, C., Foulon, H., Radulovie, S., and Roux, Ph., "Reduction of Supersonic Jet Noise. Application to the Ariane 5 Launch Vehicle," AIAA Paper June 2000-2026, 2000.

[14] Gely, D., Elias, G., Mascanzoni, F., and Foulon, H., "Acoustic Environment of the VEGA Launch Vehicle at Lift-Off," ONERA TP 2005-148, 2005.

[15] Panda, J., and Mosher, R., "Microphone Phased Array to Identify Liftoff Noise Sources in Model-Scale Tests," *Journal of Spacecraft and Rockets*, Vol.50, No.5, 2013, pp.1002-1012.

[16] Tsutsumi, S., Takaki, R., Shima, E., Fujii, K., and Arita, M., "Generation and Propagation of Pressure waves from H-IIA Launch Vehicle at Lift-off," AIAA Paper 2008-390, January 2008.

[17] Tsutsumi, S.,Fukuda, K., Takaki, R., Shima, E.,Fujii, K., and Ui, K.,"Numerical Study on Acoustic Radiation for Designing Launch-pad of Advanced Solid Rocket," AIAA Paper 2008-5148, July 2008.

[18] Tsutsumi, S., S. Kato, Fukuda, K.,Takaki, and Ui, K., "Effect of Deflector Shape on Acoustic Field of Launch Vehicle at Lift-off," AIAA Paper 2009-0328, January 2009.

[19] Nonomura, T., Goto, Y. and Fujii, K., "Aeroacoustic waves generated from a supersonic jet impinging on an inclined flat plate," *International Journal of Aeroacoustics*, 2011, Vol.10(4), pp.401-426.

[20] Nonomura, T., and Fujii, K., "POD of Aeroacoustic Fields of a Jet Impinging on an Inclined Plate," AIAA Paper 2010-4019, June 2010.

[21] Tsutsumi, S., Takaki, R., Nakanishi, Y., Okamoto, K., and Teramoto, S., "Acoustic Generation Mechanism of a Supersonic Jet Impinging on Deflectors," AIAA Paper 2014-0882, January 2014.

[22] Akamine, M, Nakanishi, Y., Okamoto, K., Teramoto, S., Okunuki, T., and Tsutsumi, S., "Experimental Study on Acoustic Phenomena of Supersonic Jet Impinging on Inclined Flat Plate," AIAA Paper 2014-0879, January 2014.

[23] Tam, C.K.W., “Mach Wave Radiation from High-Speed Jets,” *AIAA Journal*, Vol.47, No.10, 2009, pp.2440-2448.

[24] Troutt, T.R., and McLaughlin, D.K., “Experiments on the Flow and Acoustic Properties of a Moderate-Reynolds-Number Supersonic Jet,” *Journal of Fluid Mechanics*, Vol.116, 1982, pp.123-156.

[25] Maekawa, Z, “Noise Reduction by Screens,” *Applied Acoustics*, Vol.1, 1968, pp.157-173.

[26] Fukuda, K, Tsutsumi, S., Ui, K., Ishii, T., Takaki, R., and Fujii, K., “An Acoustic Impedance Model for Evaluating the Ground Effect of Static-Firing Tests on a Rocket Motor,” *Transactions of the Japan Society for Aeronautical and Space Sciences*, Vol.54, No.184, 2011, pp.120-129.

[27] Krothapalli, A., Rajkuperan, E., Alvi, F., and Lourenco, L, “Flow Field and Noise Characteristics of a Supersonic Impinging Jet,” *Journal of Fluid Mechanics*, Vol.392, 1999, pp.155-181.

[28] Sutherland, C. L., “Progress and Problems in Rocket Noise Prediction for Ground Facilities,” AIAA Paper 93-4383, October 1993.

[29] International Organization for Standardization, “Acoustics - Attenuation of sound during propagation outdoors -,” ISO9613-1, 1996.

[30] Imaizumi, H., Takahashi, Y., Isei, T., “Outdoor Sound Propagation Ranging from Hundreds to Hundreds of Thousands of Meters”, *Journal of the INCE of Japan*, Vol.28, No.4, pp.264-269, 2004. (in Japanese)

[31] Fukuda, K., Tsutsumi, S., Fujii, K., Ui, K., Ishii, T., Oinuma, H., Kazawa, J., Minesugi, K., “Acoustic Measurement and Prediction of Solid Rockets in Static Firing Tests,” AIAA Paper 2009-3368, May 2009.

[32] Tsutsumi, S., Fukuda, K., Takaki, R., Ishii, T., and Ui, K., “Acoustic Design of Launch Pad for Advanced Solid Rocket,” *Journal of Acoustical Society of America*, Vol.127, No.3, March pp.1742.

[33] Spalart P.R., and Allmaras, S.R., “A One Equation Turbulence Model for Aerodynamic Flows,” AIAA Paper 92-0439, January 1992.

[34] Shima, E., “A Simple Implicit Scheme for Structred/Unstrectured CFD,” *Proceedings of 29th Fluid Dynamic Symposium, Hokkaido, Japan*, The Japan Society for Aeronautical and Space Sciences, Tokyo, 1997, pp.325-328. (in Japanese)

[35] Kobayashi, M.H., “On a Class of Padé Finite Volume Methods,” *Journal of Computational Physics*, Vol.156, 1999, pp.127-180.

[36] Gaitonde, D.V., and Visbal, M.R., “Padé-Type Higher-Order Boundary Filters for the Navier-Stokes Equations,” *AIAA Journal*, Vol.38, No.11, 2000, pp.2103-2112.

[37] Visbal, M.R., and Gaitonde, D.V., “Shock Capturing Using Compact-Differencing-Based Methods,” AIAA Paper 2005-1265, January 2005.

[38] Shima, E., and Kitamura, K., “Parameter-Free Simple Low-Dissipation AUSM-Family Scheme for All Speeds,” *AIAA Journal*, Vol.49, No.2, 2011, pp.584-590.

[39] Lyrintzis, A.S., "Integral Acoustics Methods: From the (CFD) Near- Field to the (Acoustic) Far-field," *International Journal of Aeroacoustics,* Vol. 2, No. 2, 2003, pp. 95-128.

[40] Tsutsumi, S., Nonomura, T., Fujii, K., Nakanishi, Y., Okamoto, K., and Teramoto S., "Analysis of Acoustic Wave from Supersonic Jets Impinging to an Inclined Flat Plate," *Proceedings of International Conference on Computational Fluid Dynamic*s (ICCFD) 7, ICCFD7-3104, July 2012.

[41] Cacqueray, N., Bogey, C., and Bailly, C., "Investigation of a High-Mach-Number Overexpanded Jet Using Large-Eddy Simulation," AIAA Journal, Vol.49, No.10, 2011, pp.2171-2182.

[42] Bodony, D.J., and Lele, S.K., "Review of the Current Status of Jet Noise Prediction Using Large-Eddy Simulation (invited)," AIAA Paper 2006-486, January 2006.

[43] Nonomura, T., and Fujii, K., "Overexpansion Effects on Characteristics of Mach Waves from a Supersonic Cold Jet," AIAA Journal, Vol.49, No.10, 2011, pp.2282-2294.

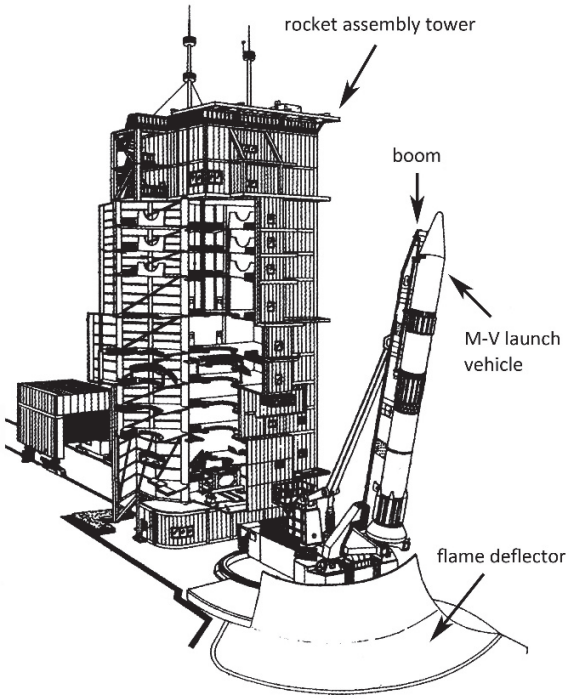

Fig. 1 Schematic of the M-V launch pad.

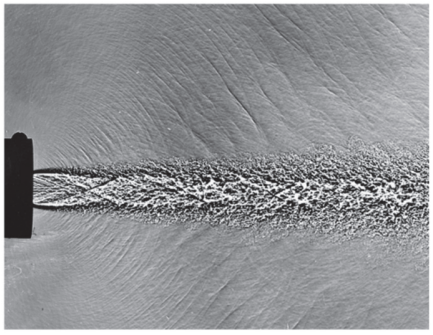

Fig. 2 Shadowgraph of a cold jet with *Me*=2.[23]

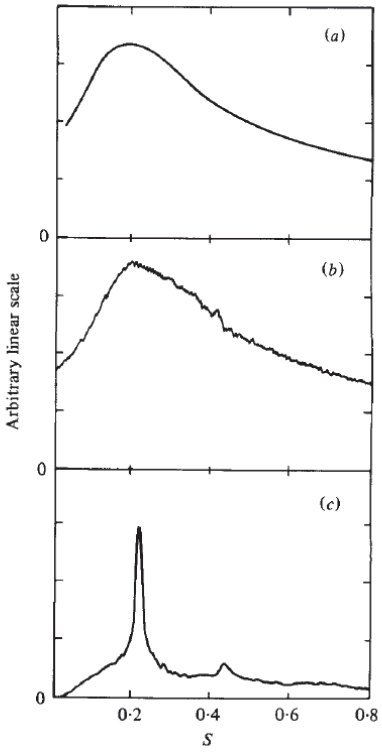

Fig. 3 Effect of the Reynolds number on the acoustic spectrum in the major acoustic-emission direction. (a) M=2.0, Re=2.6×10^6, (b) M=2.1, Re=7×10^4, (c) M=2.1, Re=7900.[3]

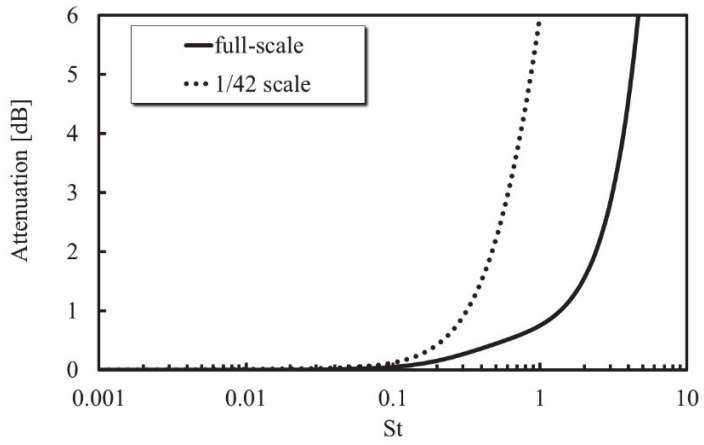

Fig. 4 Comparison of the air absorption effect between full-scale and 1/42 subscale conditions. Propagation distance is 60D_e.

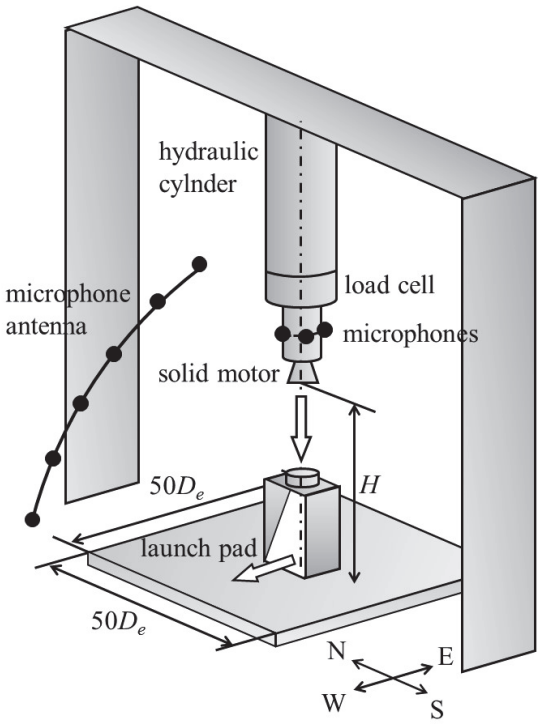

Fig. 5 Schematic of test stand.

Table 1 Jet conditions.

M_e	M_j	M_a	P_o/P_a	T_o/T_a	P_e/P_a	Re	γ_j	γ_a
3.7	3.3	8.6	89.1	12.0	0.5	2.2×10^5	1.2	1.4

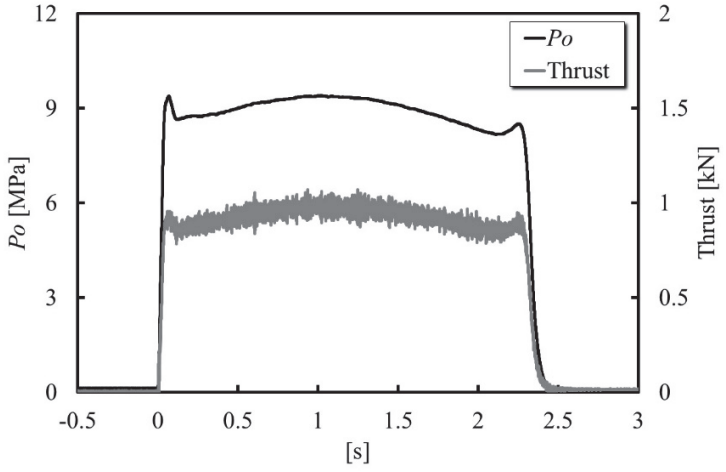

Fig.6 Time histories of chamber pressure and thrust.

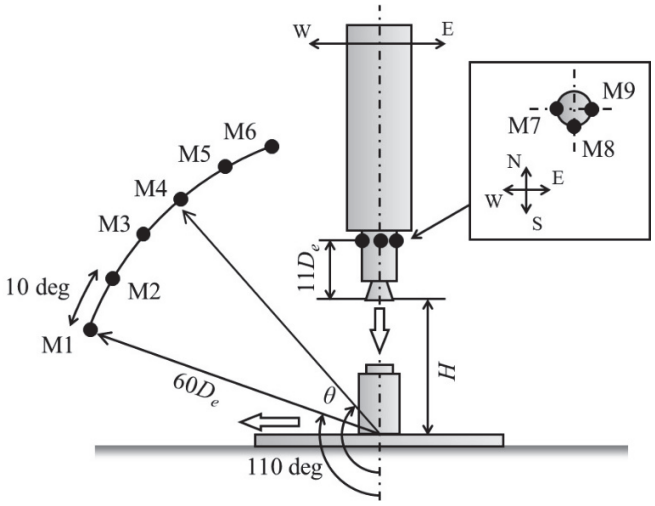

Fig. 7 Placement of microphones.

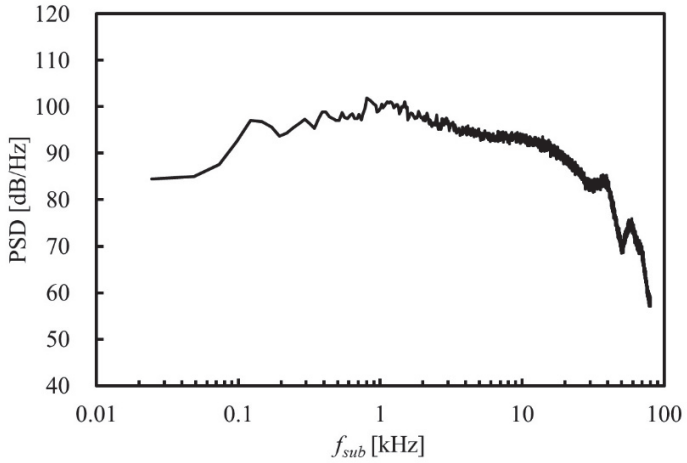

Fig. 8 Typical acoustic data.

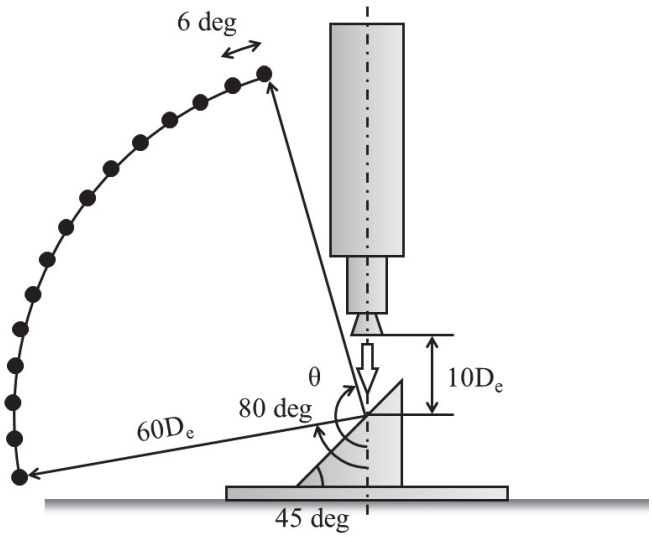

Fig. 9 Placement of microphones for measurements with a 45-degree-inclided flat plate.

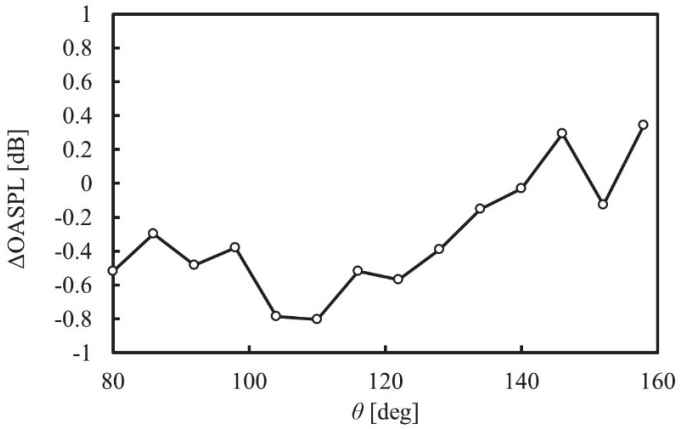

(a) OASPL.

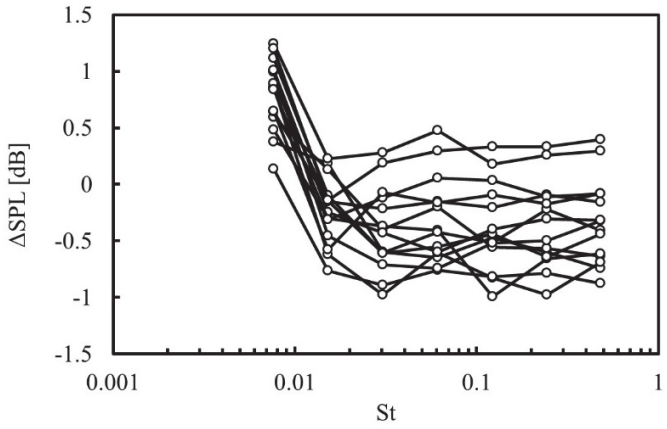

(b) 1/1 octave-band SPL at 14 microphones.

Fig. 10 Difference between two tests for checking repeatability of acoustic measurements.

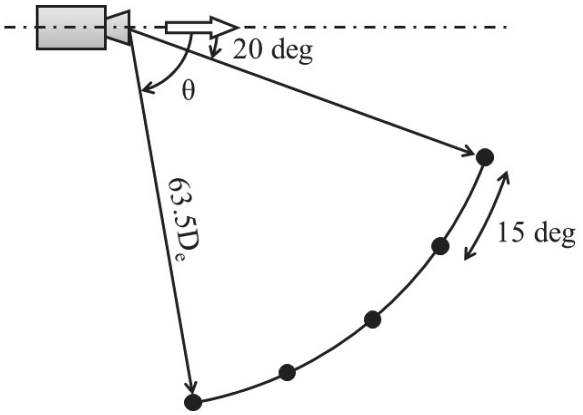

(a) 1/3 scale motor having 260-kN thrust.

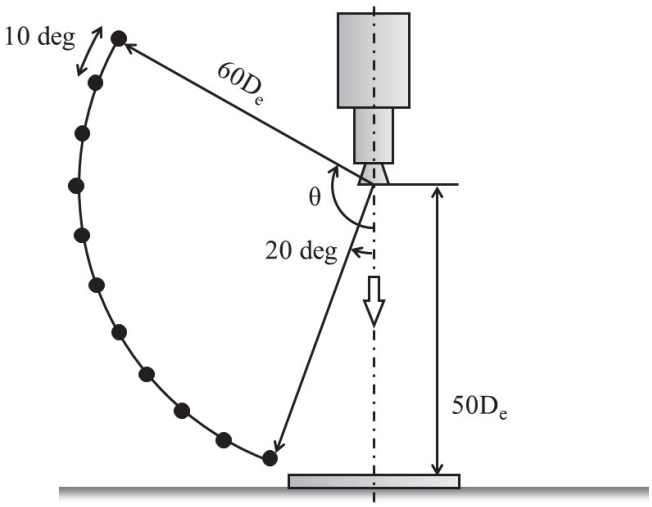

(b) 1/42 scale motor in this study.

Fig.11 Schematic of test configurations and microphone layouts for free jet measurements.

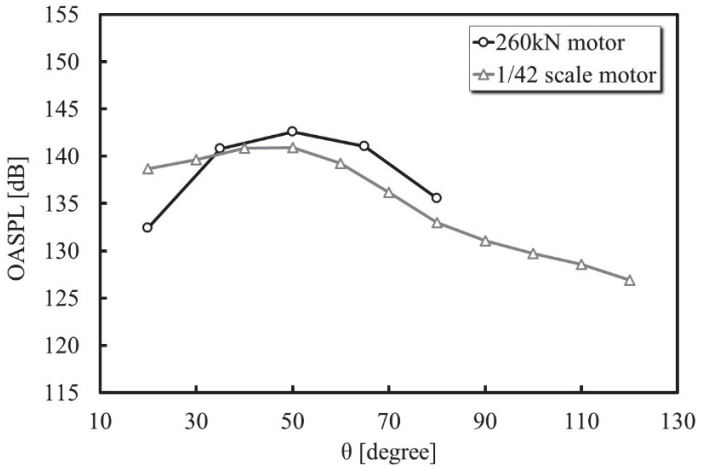

(a) OASPL.

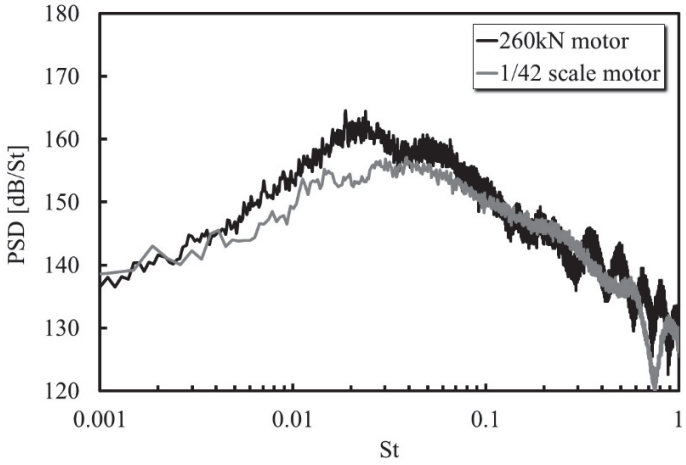

(b) PSD at θ=50 degree.

Fig. 12 Comparison of acoustic results between 260 kN solid motor and 1/42 scale motor at R=60D_e.

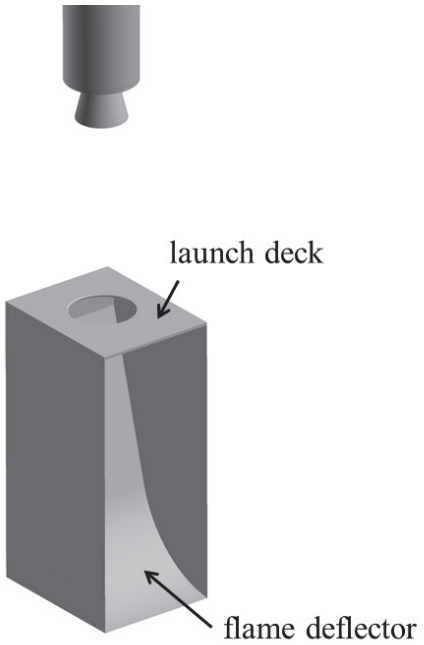

Fig. 13 Preliminary configuration.

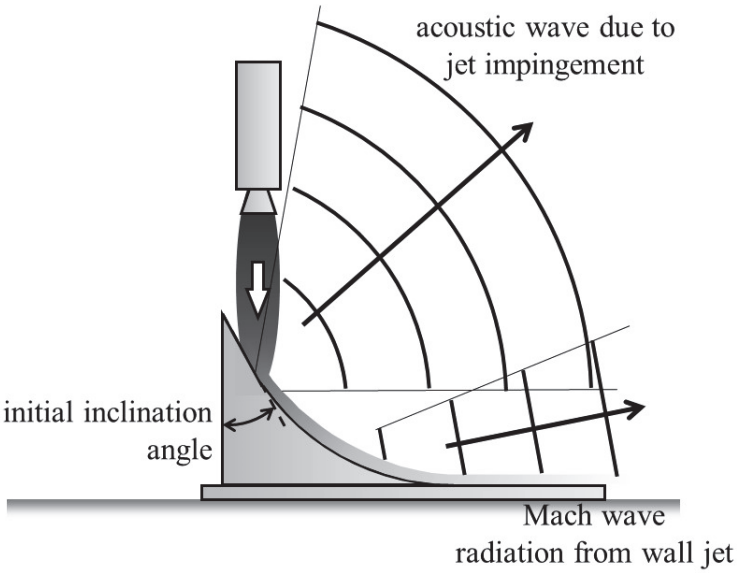

(a) Acoustic sources when the vehicle is close to deflector.

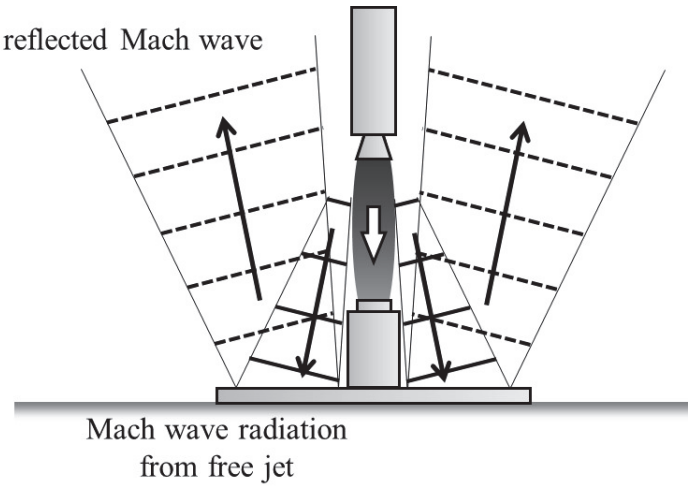

(b) Acoustic sources when the vehicle climbs.

Fig. 14 Schematic of acoustic sources.

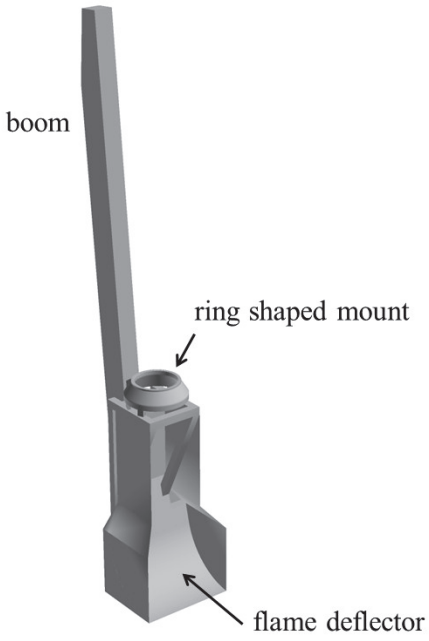

(a) Baseline configuration.

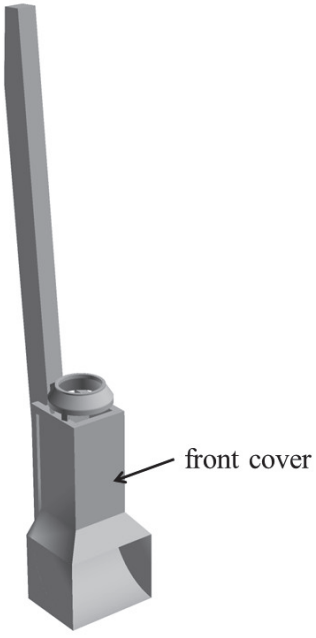

(b) Baseline configuration with front cover.

Fig. 15 Configuration of subscale launch pads.

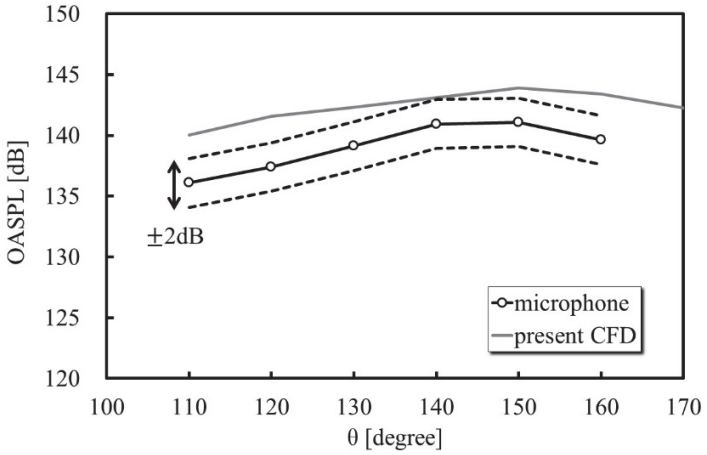

(a) OASPL plot evaluated at 0.012 < St < 0.48. Offset of measured levels by ±2 dB is shown by dashed lines.

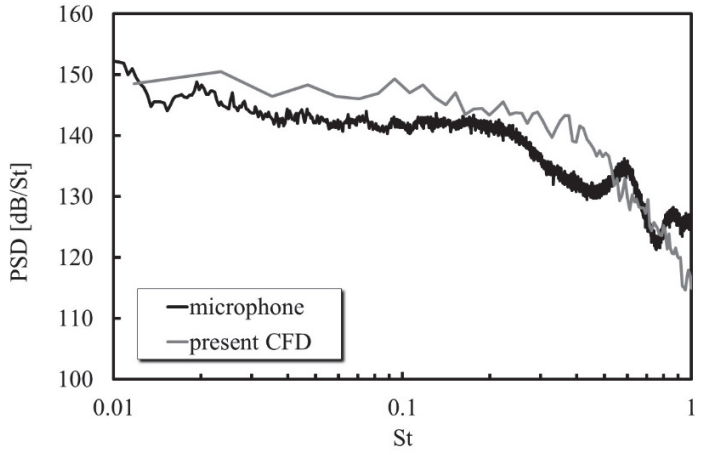

(b) PSD at M2 (θ=120 degree).

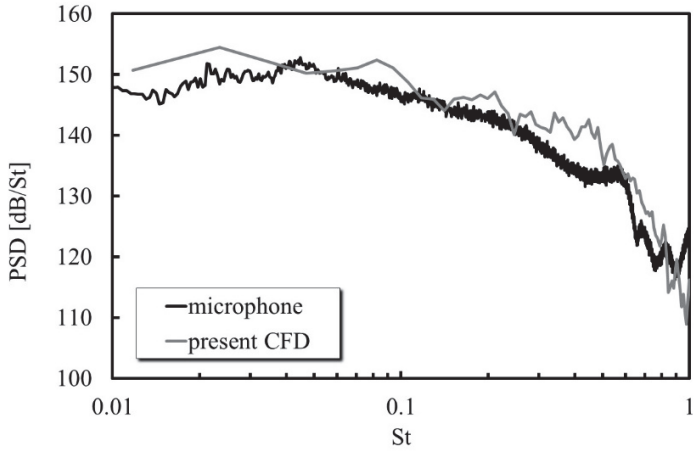

(c) PSD at M5 (θ=150 degree).

Fig.16 Comparison of microphone measurement and numerical result.

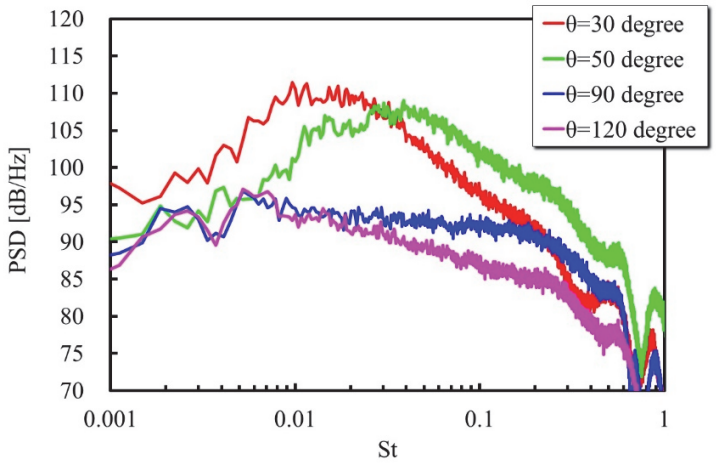

Fig. 17 PSD spectrum of free jet measured at R=60D_e microphones.

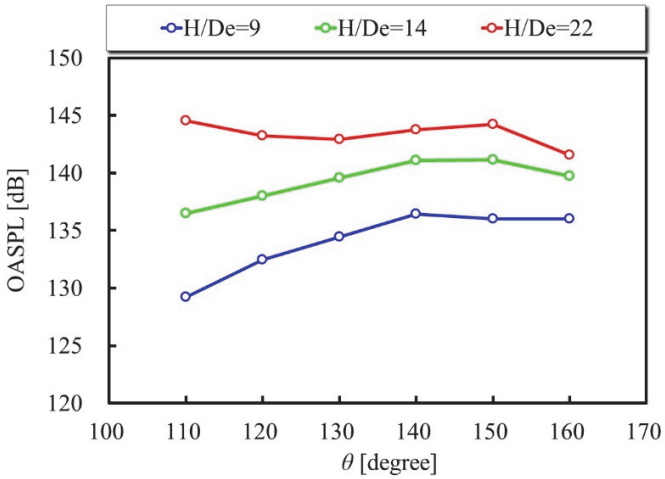

(a) OASPL.

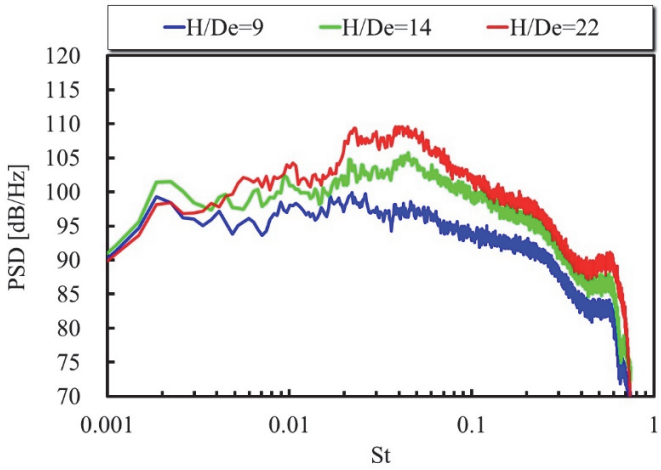

(b) PSD at θ=150 degree (M5).

Fig. 18 Effect of distance from ground on far-field acoustics.

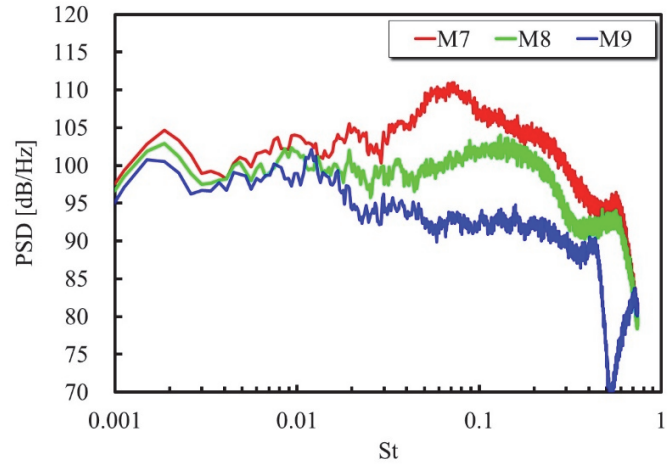

Fig. 19 Comparison of circumferential microphones at fairing location in the H/D_e=14 case.

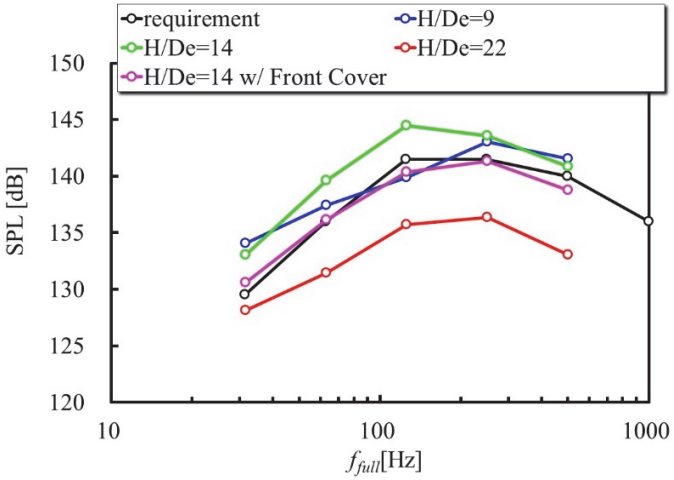

Fig. 20 Comparison of 1/1 octave-band SPL measured at M7.

Table 2 OASPL levels measured at M7.

	OASPL dB
H/D_e=9	147.7
H/D_e=14	149.1
H/D_e=22	141.3
H/D_e=14 w/ Front Cover	146.2

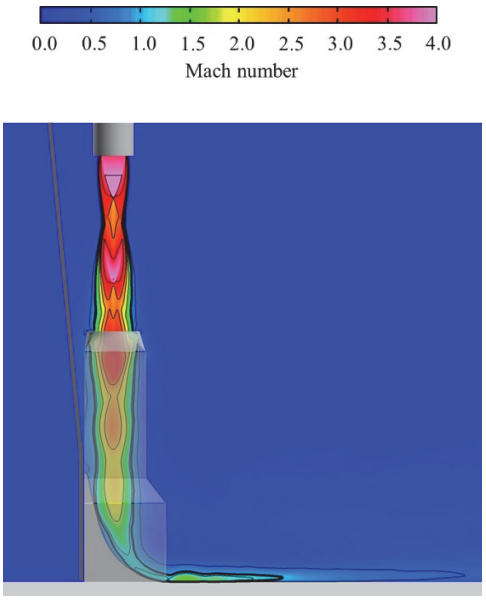

(a) Mean Mach number plot. Thick black line is the sonic line.

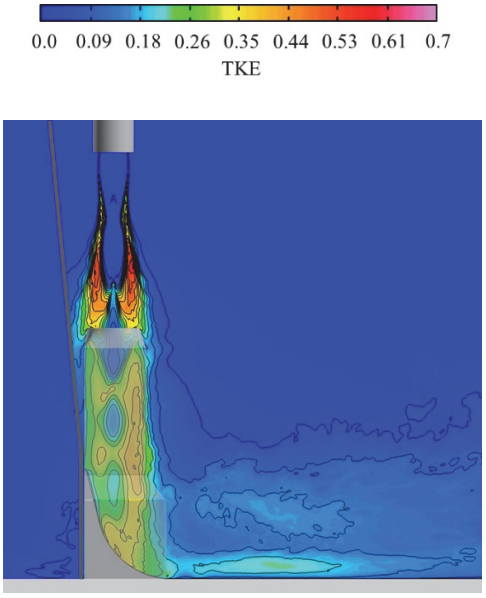

(b) Turbulent Kinetic Energy (TKE) plot.

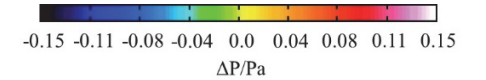

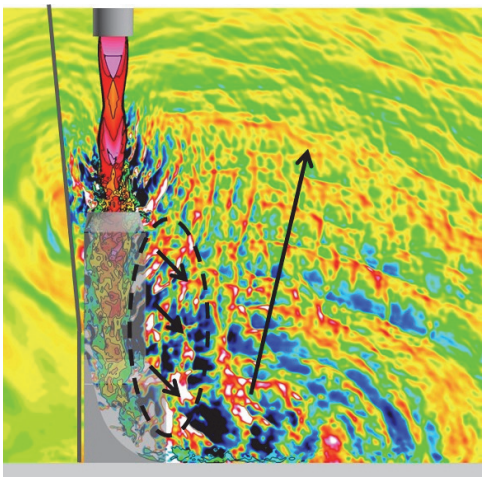

(c) Pressure plot with the jet flow visualized by Mach number.

Fig. 21 Numerical results for the baseline configuration at H/D_e=14.

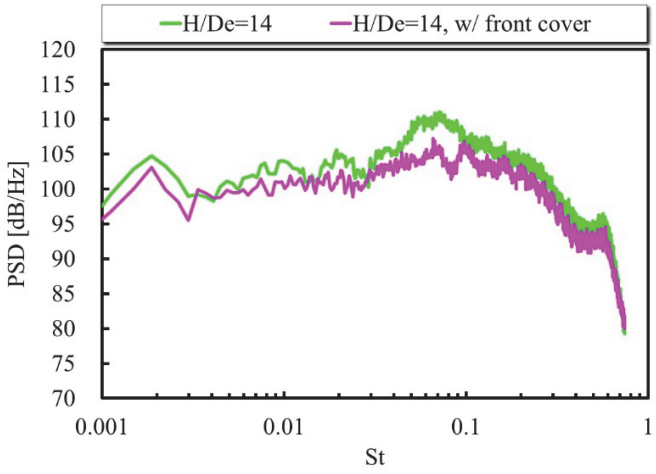

Fig. 22 Effect of the front cover at H/D_e=14.